**Atmospheric
Chemistry
and Physics**

A transboundary transport episode of nitrogen dioxide as observed from GOME and its impact in the Alpine region

D. Schaub[1], A. K. Weiss[1], J. W. Kaiser[2], A. Petritoli[3], A. Richter[4], B. Buchmann[1], and J. P. Burrows[4]

[1]Swiss Federal Lab. for Materials Testing & Research (EMPA), Ueberlandstrasse 129, CH-8600 Duebendorf, Switzerland
[2]Remote Sensing Laboratories, University of Zurich, Winterthurerstrasse 190, CH-8057 Zurich, Switzerland
[3]Institute of Atmospheric Science and Climate (ISAC-CNR), Via Gobetti 101, I-40129 Bologna, Italy
[4]Institute of Environmental Physics, University of Bremen, P.O. Box 33 04 40, D-28334 Bremen, Germany

Abstract. High tropospheric NO_2 amounts are occasionally detected by space-borne spectrometers above cloudy scenes. For monitoring of near-ground air pollution such data are not directly applicable because clouds shield the highly polluted planetary boundary layer (PBL). We present a method based on trajectories which implicitly estimates the additional sub-cloud NO_2 distribution in order to model concentrations at ground stations. The method is applied to a transboundary pollution transport episode which led to high NO_2 vertical tropospheric column densities (VTCs) over middle Europe observed by the Global Ozone Monitoring Experiment (GOME) instrument above clouds on 17 February 2001. The case study shows that pollution originally residing near the ground in central Germany, the Ruhr area and adjacent parts of the Netherlands and Belgium has been advected to higher tropospheric levels by a passing weather front. Combining the above-cloud NO_2 VTCs with trajectory information covering the GOME columns and including their sub-cloud part yields an estimate of the total NO_2 distribution within the tropospheric columns. The highly polluted air masses are then traced by forward trajectories starting from the GOME columns to move further to the Alpine region and their impact there is assessed. Considering ground-based in-situ measurements in the Alpine region, we conclude that for this episode, at least 50% of the NO_2 concentration recorded at the sites can be attributed to transboundary transport during the frontal passage. This study demonstrates the potential of using NO_2 VTCs from GOME detected above clouds when combined with transport modelling.

1 Introduction

Nitrogen dioxide (NO_2) plays a key role in photochemical air pollution. Its amount and distribution is of significance directly for air quality and human health and indirectly as an ozone precursor (e.g. Seinfeld and Pandis, 1998). Therefore, for air quality policy, accurate source attribution and impact assessment is required.

1.1 NO_2 chemistry

NO_2 is formed according to the photochemical equilibrium on a time scale of minutes from the primarily emitted nitrogen oxide (NO), the bulk of which is of anthropogenic origin (Brasseur, 2003). The NO_2 concentration at any time and place is determined by the emission of NO_x ($\equiv NO+NO_2$), its production and loss reactions as well as meteorological transport and dilution. Furthermore, the NO_2 concentration is affected by the partitioning of NO_x into NO and NO_2 which depends on the meteorological conditions, the abundance of reactive organic compounds and the altitude in the troposphere. During the Transport and Chemical Evolution over the Pacific (TRACE-P) campaign between February and April 2001 (Jacob et al., 2003), the bulk of the NO/NO_2 ratios have been found to be around 0.25 at near-ground levels (Nakamura et al., 2003). Similar values from different campaigns can be found in Warneck (2000). Ratios of up to 1 are found in the middle troposphere (Nakamura et al., 2003).

NO_2 is removed from the troposphere through conversion to nitric acid (HNO_3) which deposits (Kramm et al., 1995). During daytime, HNO_3 emanates from the reaction of NO_2 with the OH radical. During night time, NO_2 reacts with ozone to form the NO_3 radical, the latter further reacting with NO_2 to N_2O_5. Nitrogen pentoxide subsequently reacts on surfaces and aerosol to HNO_3 (Dentener and Crutzen, 1993). Although diurnal variations of the NO_2 lifetime are

Correspondence to: D. Schaub
(daniel.schaub@empa.ch)

considerable and may be only a few hours during photochemically active summer days, the average boundary layer lifetime during the whole year is estimated to be in the order of one day (Warneck, 2000). Leue et al. (2001) used vertical tropospheric NO_2 column densities observed from GOME over the eastern coast of North America to estimate an NO_2 lifetime of 27 hours in the planetary boundary layer (PBL). Following the plume leaving the coast of India, Kunhikrishnan et al. (2004) estimated a lifetime of 18 h. However, in the middle and upper troposphere, decreasing OH and aerosol concentrations lead to a longer NO_2 lifetime being of the order of several days to a week (Jaeglé et al., 1998; Seinfeld and Pandis, 1998; Warneck, 2000). Thus, NO_2 may be transported over larger distances once it is lifted to higher tropospheric levels, for example by frontal systems.

1.2 Previous observations

For high-alpine sites, the importance of meteorological transport processes such as frontal advection on the variability of trace gases has been shown. For example, Forrer et al. (2000) investigated among others the variability of NO_x at the high-alpine site Jungfraujoch and found that during such events, NO_x concentrations can increase from below 1 ppb up to around 10 ppb. Such frontal episodes have been found to significantly increase the monthly mean concentrations during the whole year, most pronounced during winter months. Further investigations at our institute have distinguished between background and polluted conditions at the high-alpine site Jungfraujoch based on classifying trajectories. It has been found that around one third of the days at this site are affected by synoptical lifting and frontal pollution transport causing an average NO_x concentration increase in the order of 100%.

Numerical model results have shown synoptic-scale vertical advection to be a significant transport mechanism for nitrogen oxides (Hov and Flatoy, 1997). In agreement with this, more than 50% of a passive tracer released in the boundary layer was found to be transported to the free troposphere within 24 h during a frontal passage (Donnell et al., 2001). Aircraft campaigns have verified that significant quantities of trace gases are lifted up from the PBL into the free troposphere by a warm conveyor belt associated with the frontal system (Bethan et al., 1998). The importance of synoptic uplift and subsequent long-range transport of trace gases for air pollution monitoring was shown by Stohl et al. (2002).

The retrieval of the tropospheric NO_2 column from spaceborne instrumentation has become available since the launch of the GOME instrument (Burrows et al., 1999) aboard the European Space Agency (ESA) satellite ERS-2 (Earth Remote Sensing Satellite). GOME measurements were successfully used to observe intercontinental transport events of nitrogen dioxide (Spichtinger et al., 2001; Wenig et al., 2003; Stohl et al., 2003). Therefore, combining satellite and ground-based data with transport models is useful to observe transport phenomena influencing the NO_2 distribution.

1.3 Present study

We present a method to quantify air pollution transport based on trajectory analysis by using tropospheric NO_2 observed from GOME above clouds instead of emission inventories. The method is applicable for high NO_2 columns observed from GOME above an extended cloud cover where lightning NO_x can be excluded and, thus, a frontal transport episode is postulated to have advected near-ground pollution above the cloud cover. Because the trajectories cover the whole GOME column including its sub-cloud part, the method implicitly estimates the NO_2 distribution within the whole column.

In this paper, an episode of "intracontinental" transport of nitrogen dioxide is investigated for a cloudy scene on 17 February 2001. First, the source region of the pollution detected from GOME is assessed with backward trajectories. Forward trajectories are used to estimate potential impact regions of the pollution transport. Employing a higher number of trajectories and the GOME NO_2 VTCs the NO_2 transport and its impact in the Alpine region is identified quantitatively and compared to ground-based in-situ measurements.

2 Measurement data

2.1 GOME measurements

The GOME instrument aboard ESA's ERS-2 satellite measures upwelling radiance from the atmosphere and extraterrestrial solar irradiance. The amount and distribution of a variety of significant atmospheric trace constituents may be retrieved from these observations (Burrows et al., 1999). It was designed and optimised primarily to measure the global ozone distribution, but also the amounts of the trace gases BrO, OCIO, H_2O, HCHO and NO_2 can be obtained.

The GOME instrument comprises a nadir-viewing spectrometer which observes simultaneously the entire spectral range between 240 and 793 nm at channel dependent spectral resolutions between 0.2 and 0.4 nm. From the spectral features of the trace gases, their vertical columns are retrieved (e.g. Richter and Burrows, 2002). Because of its sun-synchronous polar orbit, GOME measurements in middle latitudes are always taken in the late morning local time. With its swath width of 960 km (single ground pixel size is 320 km across track and 40 km along track) GOME reaches full coverage at the mid-latitudes within 2–3 days.

The NO_2 vertical tropospheric column density (VTC) data used in this study were provided by the University of Bremen (Richter and Burrows, 2002). Uncertainties in the VTCs are due to the NO_2 fitting algorithm, instrument characteristics, the method of the stratosphere-troposphere separation and atmospheric parameters such as the a priori NO_2 profile shape, the surface spectral reflectance, the aerosol loading and the

clouds. These atmospheric parameters account for the largest part of the uncertainties. Richter and Burrows (2002) and Boersma et al. (2004) carried out detailed error analysis for the NO_2 VTCs and found a total uncertainty of up to a factor of 2. In order to reduce the uncertainty, the GOME data used in the present study were reprocessed with an adapted cloud top height (CTH) and an assumed location of the NO_2 layer. Furthermore, different scenarios for the structure of the cloud cover (closed cloud cover and partly cloudy taking into account cloud mask data) are used.

2.2 Ground-based in-situ measurements

The Swiss National Air Pollution Monitoring Network (NABEL) provides long-term ambient air measurements (EMPA, 2002; BUWAL, 2002). To investigate the impact of the mesoscale transport process, rural and remote sites located in the Swiss Plateau or elevated and north-exposed stations are suitable as the air mass inflow during this episode is from northern to north-eastern direction.

Data from the following sites (Fig. 1) are used in this study:

A) Rigi (47°04′ N, 8°28′ E, 1030 m a.s.l.):
A rural site that is well suited for detection of events advected from northern direction, because it is situated on a north-exposed mountain slope. In winter, local influences arising from thermal transport are rare.

B) Chaumont (47°03′ N, 6°59′ E, 1140 m a.s.l.):
This site is also situated at an elevated location at some distance from cities and is surrounded by meadows and grassland. The nearest industrial enterprises are situated 5 to 10 km away.

C) Taenikon (47°28′ N, 8°54′ E, 540 m a.s.l.):
A site that samples air from the Swiss Plateau. The surroundings are dominated by agriculture and forests, the highway A1 lies in north-eastern direction at a distance of 4 km.

D) Zugspitze (47°25′ N, 10°59′ E, 2963 m a.s.l.):
This site is located at the northern rim of the Alps and, therefore, suitable for the detection of air masses advected from the North (Umweltbundesamt, 2002). It is used because no measurements from the high-alpine site Jungfraujoch (Switzerland) are available during the time of the case study.

At these sites, nitrogen oxides are measured with the ozone chemiluminescence detectors Monitor Labs (ML) 8841 (Rigi), ML 9841 A (Chaumont), ECO Physics CLD 700 (Taenikon) and TE 42 Thermo Environmental Systems/TECAN (Zugspitze). All measurement devices are equipped with a molybdenum converter. It should be noted that these catalytic surface converters are sensitive not only to NO_2, but also to other nitrogen species such as PAN, HNO_2,
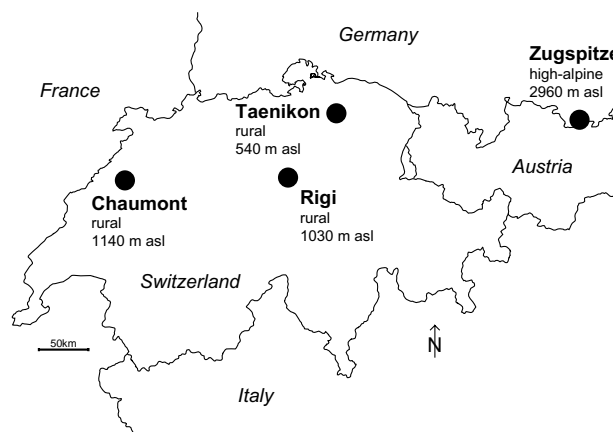

Fig. 1. The location of the three remote ground-based measurement stations operated by the Swiss National Air Pollution Monitoring Network (NABEL) and the Zugspitze station (Umweltbundesamt, 2002) which are used in this case study.

HNO_3 and particulate nitrate to NO. Generally, the PAN mixing ratio can be expected to be small during winter conditions. Wunderli and Gehrig (1991) found a mean February PAN mixing ratio at Davos (Switzerland, 1640 meters asl) of 0.1 ppb. Under cold and clear weather conditions, however, elevated PAN mixing ratios were measured in winter with an evening maximum at Davos of 0.6 ppb. HNO_2 is rapidly transformed to OH and NO by photolysis and mixing ratios are normally below the detection limit during the day (Winer and Biermann, 1994). Maximum February/March HNO_3 concentrations were found to be in the order of 0.3 ppb at Jungfraujoch (Zellweger et al., 2003) and 0.8 ppb in Duebendorf (Zellweger et al., 1999) at 3580 m a.s.l. and 430 m a.s.l., respectively. Particulate nitrate exhibits large temporal and spatial variations and might have the strongest influence on the interference. In March 1997, Zellweger et al. (1999) measured nitrate concentrations of up to 5.5 ppb at the Swiss Plateau station Duebendorf. February measurements at the high-alpine site Jungfraujoch indicated maximum concentrations of 0.3 ppb during weak thermal transport events and much lower values when thermal transport is absent (Zellweger et al., 2003). As the NO_2 mixing ratios are between 5 (high-alpine) and 30 ppb (Swiss Plateau) in this case study, we consider the interference of the above discussed nitrogen species to have a minor influence.

3 Methods

3.1 Trajectory calculations

Backward and forward trajectories are used to investigate the origin of the detected air masses in the studied GOME columns and their further movement. The trajectories are

based on analysed wind fields with a six hour temporal and $1° \times 1°$ geographical resolution provided by the model of the European Centre for Medium-Range Weather Forecast (ECMWF). Three dimensional kinematic backward and forward trajectories are calculated with the software package "Lagranto" (Wernli and Davies, 1997). Their length is chosen to be long enough for source and impact analysis (several days). The NO$_2$ distribution within the GOME columns is unknown. Therefore, the backward/forward trajectory arrival/starting points cover the GOME columns both horizontally and vertically in order to account for its whole tropospheric volume ($320 \, \text{km} \times 40 \, \text{km} \times$ tropopause height).

For a first assessment of the source regions and the further air mass movement (Sects. 4.3 and 4.4), each column is covered with 70 arrival/starting points; 10 levels from 900 hPa up to 400 hPa in 50 hPa steps, each level containing 7 points. For a quantitative transport assessment (Sects. 3.2 and 4.6), a much higher density of backward and forward trajectories is calculated for each GOME column with 128 (4 along track $\times$ 32 across track) arrival/starting points in the horizontal for 23 height levels between 950 hPa and 400 hPa in 25 hPa steps (resulting in a total of 2944 trajectories per column). The arrival/starting time point for the case study is chosen to be on 17 February 2001, 9:00 UTC corresponding to the GOME overpass at around 10:15 local time.

3.2 Transport model based on trajectories and GOME observations

A transport model based on backward and forward trajectories, GOME NO$_2$ VTCs above a cloudy scene, population distribution data, and an assumed average NO$_2$ lifetime is employed to estimate the amount of advected NO$_2$ at ground measurement sites. The method comprising three steps is discussed in detail in the following sections and is illustrated in Fig. 2. Firstly, the population number is added up (as a proxy for NO$_2$ emissions), transported along the backward trajectories and corrected for the NO$_2$ lifetime (Sect. 3.2.1). Secondly, the NO$_2$ proxy arriving in the GOME columns is summed vertically above different CTH. These proxy VTCs are compared to the GOME NO$_2$ VTCs in order to identify an effective CTH (CTH$_{eff}$) where the modelled above-cloud pollution best reproduces the detected pollution from GOME. Relating the proxy VTCs above CTH$_{eff}$ to the GOME NO$_2$ VTCs yields a conversion factor. Using the latter, the proxy is converted to number of NO$_2$ molecules (Sect. 3.2.2). Thirdly, the NO$_2$ polluted air masses is traced with forward trajectories, corrected for the NO$_2$ lifetime and converted into NO$_2$ mixing ratios when trajectories reach near-ground levels (Sect. 3.2.3).

3.2.1 Pollution uptake and NO$_2$ lifetime correction

The NO$_2$ uptake along the backward trajectories is simulated by passing the trajectories over a $1° \times 1°$ resolved popula-

tion grid (UNEP: Global Population Distribution Database, http://grid2.cr.usgs.gov/globalpop, 1997) assuming the NO$_2$ emission to be proportional to the population in the respective grid cell. Following the trajectory forward in time, pollution is taken up when the trajectory reaches a near-ground level of less then an assumed PBL height above model ground. In this case, the number of the population in the respective grid cell is added up along the trajectory as a proxy for NO$_2$ emissions. In order to account for the enhanced NO$_x$ emissions during daytime, the night time uptake is weighted with a factor of 0.5, whereas the daytime uptake is multiplied with a factor of 1.5. Further, the NO$_2$ proxy transported along the trajectory is decreasing every time step according to an assumed average NO$_2$ lifetime.

It must be mentioned that the bulk of NO$_x$ is emitted as NO. Further, the partitioning of NO$_x$ into NO and NO$_2$ is dependent on the meteorological conditions (and therefore the season), the pollution situation and the abundance of reactive organic compounds shifting the photostationary steady state (Warneck, 2000, and references therein). Nevertheless, we henceforth allude to NO$_2$ (emissions), because the NO$_x$ partitioning is – due to the conversion described in Sect. 3.2.2 – circumstantial for the further analysis shown here. Thus, the implicit assumptions are made that (i) emission sources are similar concerning the NO$_x$ partitioning and that (ii) the NO$_x$ partitioning during the investigated episode is similar within the transported air parcels.

3.2.2 Conversion of NO$_2$ proxy to number of NO$_2$ molecules

Each backward trajectory arrives in its appropriate GOME column containing a population number as a proxy for NO$_2$. This quantity is converted to a number of NO$_2$ molecules by applying a conversion factor. The latter is deduced from relating the sum of the considered GOME NO$_2$ VTCs detected above the clouds to the appropriate sum of the proxy VTCs above the cloud cover. As in this way also the NO$_2$ proxy below the clouds is converted, this step implicitly estimates the NO$_2$ distribution within the whole column including its sub-cloud part. However, two main issues complicate this approach:

1. The sensitivity of the GOME instrument for NO$_2$ within the column is not constant. For a cloudy pixel, the sensitivity is maximal at the CTH and decreases for NO$_2$ situated above or within the cloud (Hild et al., 2002).

2. Near-ground trajectories based on a $1° \times 1°$ resolved wind field might not properly reproduce the (frontal) air mass movement.

This prevents the straightforward use of the real CTH above which the proxy VTCs can be calculated. To account for both, we define a CTH$_{eff}$ where the modelled above-cloud pollution (proxy VTCs) best reproduces the pollution pattern
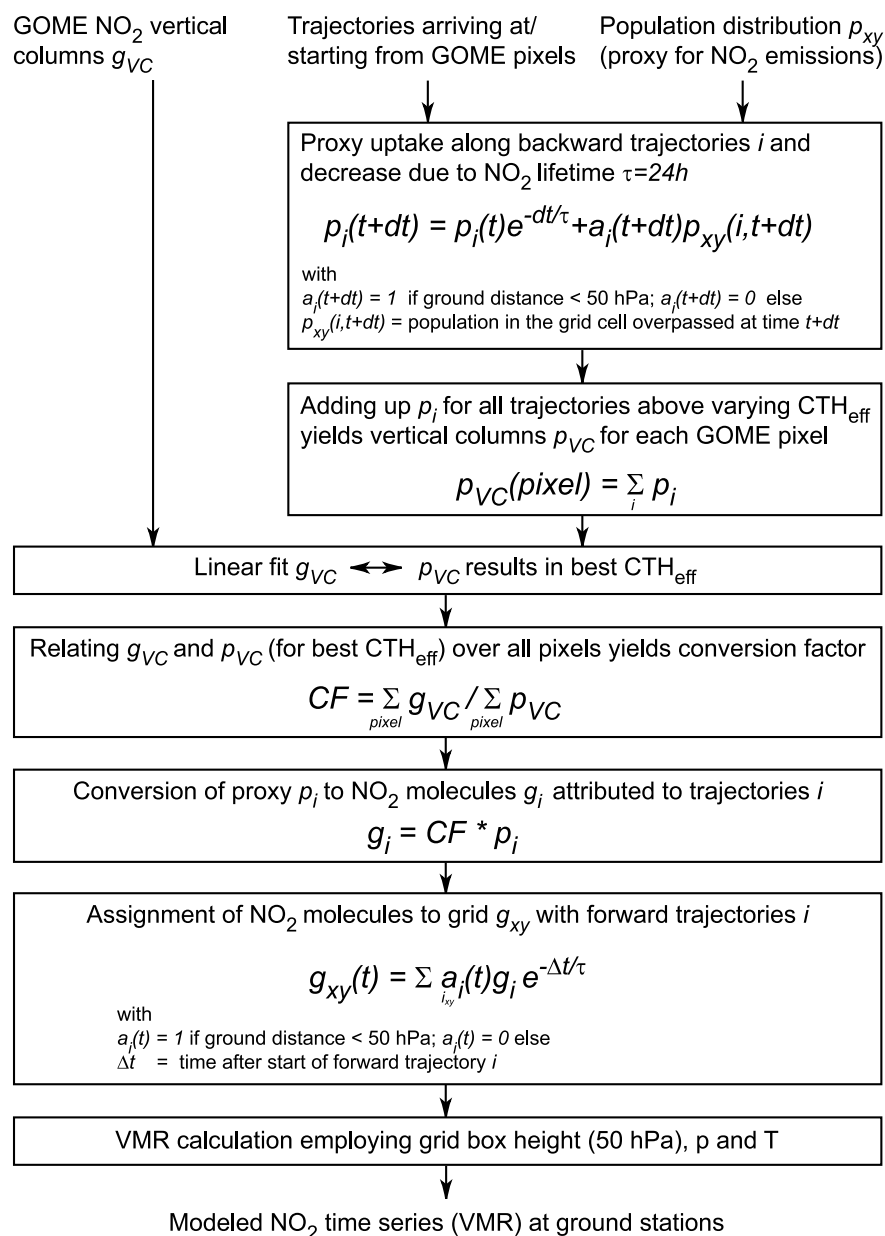
GOME NO$_2$ vertical columns g_{VC} | Trajectories arriving at/ starting from GOME pixels | Population distribution p_{xy} (proxy for NO$_2$ emissions)

Proxy uptake along backward trajectories i and decrease due to NO$_2$ lifetime $\tau=24h$

$$p_i(t+dt) = p_i(t)e^{-dt/\tau}+a_i(t+dt)p_{xy}(i,t+dt)$$

with
$a_i(t+dt) = 1$ if ground distance < 50 hPa; $a_i(t+dt) = 0$ else
$p_{xy}(i,t+dt) =$ population in the grid cell overpassed at time $t+dt$

Adding up p_i for all trajectories above varying CTH$_{eff}$ yields vertical columns p_{VC} for each GOME pixel

$$p_{VC}(pixel) = \sum_i p_i$$

Linear fit $g_{VC} \longleftrightarrow p_{VC}$ results in best CTH$_{eff}$

Relating g_{VC} and p_{VC} (for best CTH$_{eff}$) over all pixels yields conversion factor

$$CF = \sum_{pixel} g_{VC} / \sum_{pixel} p_{VC}$$

Conversion of proxy p_i to NO$_2$ molecules g_i attributed to trajectories i

$$g_i = CF * p_i$$

Assignment of NO$_2$ molecules to grid g_{xy} with forward trajectories i

$$g_{xy}(t) = \sum_{i_{xy}} a_i(t)g_i\, e^{-\Delta t/\tau}$$

with
$a_i(t) = 1$ if ground distance < 50 hPa; $a_i(t) = 0$ else
Δt = time after start of forward trajectory i

VMR calculation employing grid box height (50 hPa), p and T

Modeled NO$_2$ time series (VMR) at ground stations

Fig. 2. Flow chart illustrating the proposed method (Sect. 3.2) to model NO$_2$ mixing ratios at ground, employing population numbers assigned to the trajectories and subsequent conversion with GOME NO$_2$ vertical tropospheric column densities (VTCs). (CTH$_{eff}$=effective cloud top height, VMR=volume mixing ratio, VC=vertical column, pixel=GOME pixel).

detected from GOME (NO$_2$ VTCs). Because GOME sees to some extent into the clouds, the CTH$_{eff}$ is expected to be lower than the real CTH. The CTH is assumed to be constant across the considered GOME pixels (Fig. 3c). Linearly fitting the proxy VTCs above different CTHs with the real GOME NO$_2$ VTCs yields the adequate CTH$_{eff}$ where the explained variance R^2 maximizes.

3.2.3 Pollution propagation, NO$_2$ lifetime and conversion to NO$_2$ mixing ratios at ground stations

The NO$_2$ is modelled to propagate further along the forward trajectories. Again, the NO$_2$ loading is decreasing every time step according to the assumed average NO$_2$ lifetime. As soon as the trajectories reach near-ground levels, the impact on the NO$_2$ concentration there can be assessed by assigning the NO$_2$ values of the trajectories to appropriate grid cells superimposed over the region of interest (for the investigated
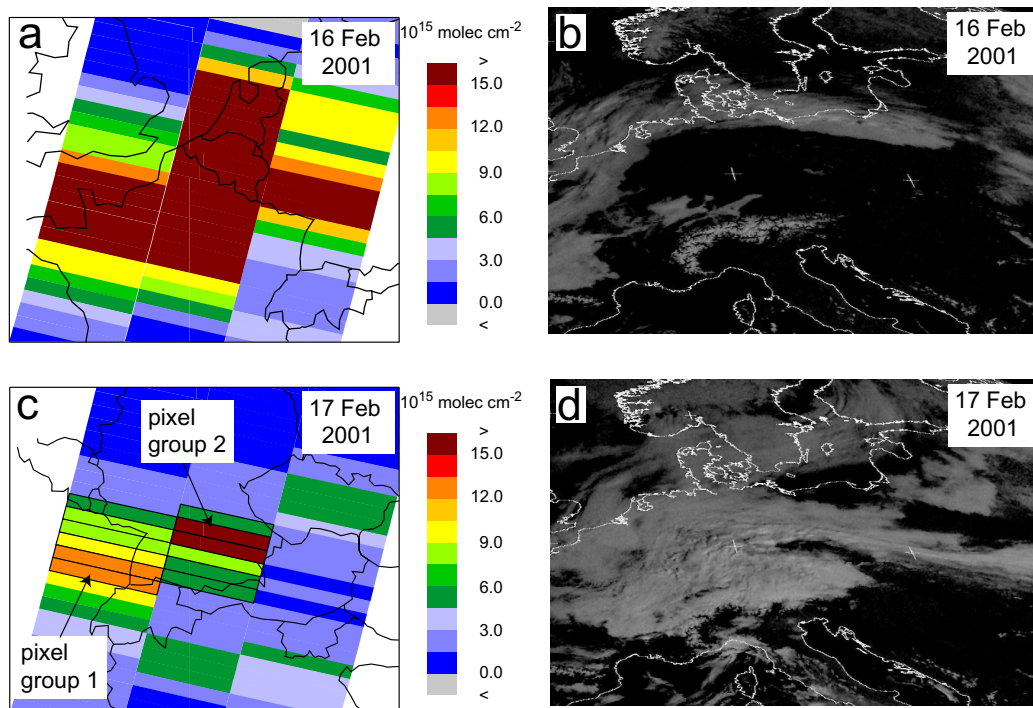
Fig. 3. (a) GOME track on 16 February, 2001, indicating high NO_2 VTCs over France, Belgium, the Netherlands and Germany. **(b)** Meteosat visible wavelength image detected at 9:30 am UCT on 16 February, 2001. **(c)** GOME track on 17 February, 2001, showing high NO_2 VTCs above clouds. For the highest values (pixel groups 1 and 2, each consisting of 2 GOME pixels) trajectories are discussed qualitatively. The transport model calculation is based on all of the 12 framed pixels found relevant for the investigated air mass. **(d)** Meteosat visible wavelength image detected at 9:30 am UTC on 17 February, 2001, indicating the extended cloud cover over middle Europe.

episode a $0.5° \times 0.5°$ resolved grid is superimposed over the Alpine region). In a last step, the hourly resolved numbers of molecules in the grid cells corresponding to the measurement sites are recalculated to mixing ratios using temperature and pressure data and the vertical box extension. The vertical box extension (near-ground level) for the case study is defined in Sect. 4.6.2.

3.2.4   Errors of the method

Main error sources of the described approach are (i) the assumption of an average lifetime of NO_2, (ii) the fact that a single air mass trajectory does not implicitly account for dilution, (iii) the error associated with the assumption of the population distribution being a representative proxy for NO_x emissions, (iv) the assumption of a constant CTH and (v) the uncertainties in the GOME NO_2 VTCs.

(i) Assuming an average lifetime for NO_2 is a strong simplification given its complex atmospheric chemistry. Especially when transport occurs within a shorter time scale (within a few hours only), also differences between daytime and night time NO_2 chemistry have to be considered. For the present case study investigating a transport episode of several days an average NO_2 lifetime is assumed. In order to account for errors arising from this simplification, the sensi-

tivity of the results with respect to the lifetime is tested (and no major impact is found, see Sect. 4.6.2). A relatively long lifetime (24 h) is chosen because the photolysis is relatively weak in winter due to the increased solar zenith angle (Dickerson et al., 1982; Parrish et al., 1983; Wiegand and Bofinger, 2000). Furthermore, the loss of NO_2 through conversion with OH to HNO_3 is slow because the amount of OH is low in winter (Seinfeld and Pandis, 1998). An average lifetime of one day can also be found in literature (Warneck, 2000) and is confirmed from assessments with tropospheric NO_2 columns from GOME (Leue et al., 2001; Kunhikrishnan et al., 2004).

(ii) The dilution is to some extent taken into account by the large number of trajectories and their divergence. Furthermore, the effect of dilution can be expected to be rather weak for the frontal transport as it lifts up an extended air mass having enhanced NO_2 concentrations and, thus, relatively small concentration gradients.

(iii) A basic assumption is that the population distribution constitutes a proxy for NO_x emissions. This seems plausible taking into account the fact that NO_x is mainly of anthropogenic origin (Brasseur et al., 2003). Although NO_x emissions along highways also take place outside the population centres, this error is expected to be of minor influence
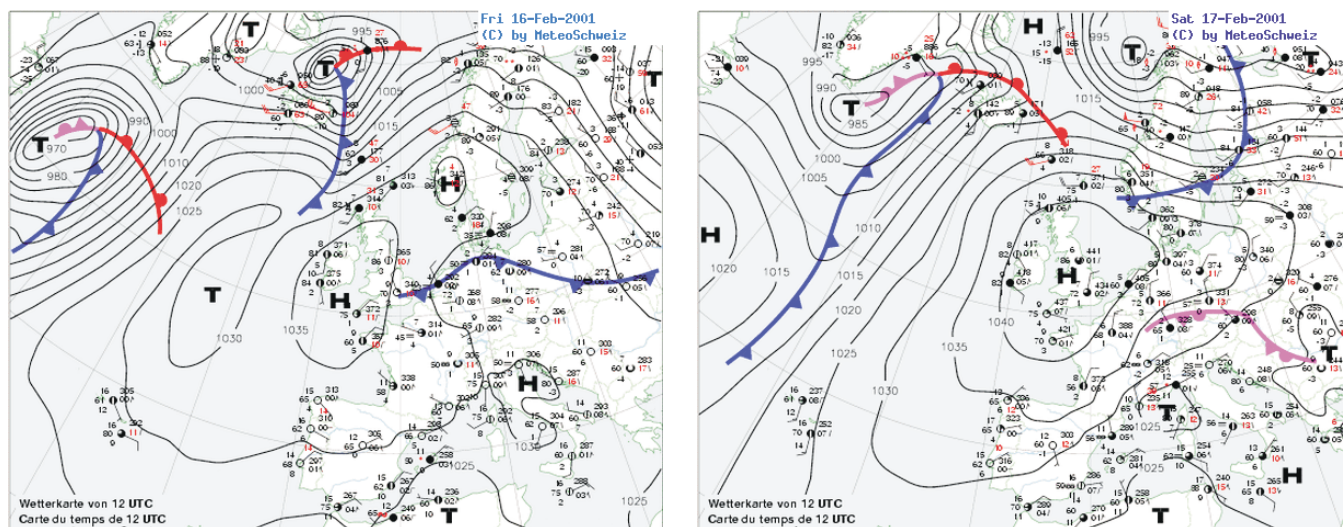
Fig. 4. Weather maps showing the southward moving cold front on 16 February 2001 (left) developing into an occlusion on 17 February (right) approaching the Alpine region.

because the population data are based on a relatively coarse resolved grid. This means that busy highways can be thought to be located around the population centres.

(iv) The CTH is essential for the described method and large inhomogeneities in the CTH must be considered. For the present study, the inspection of recent satellite data (KNMI, personal communication) indicates a rather uniform cloud cover over the considered GOME pixels and therefore, in this study, the assumption of a constant CTH is made.

(v) The error of the GOME NO_2 VTCs can be reduced by reprocessing the data considering the occurrence of clouds.

4 Case study – results and discussion

4.1 GOME observation on 17 February 2001

GOME recorded high NO_2 VTC values over central Europe on 17 February, 2001 (Fig. 3c). As can be seen in the Meteosat image (Fig. 3d), clouds shielded the ground. Therefore, a significant amount of nitrogen dioxide has to be located within and/or above the cloud cover. However, as pointed out by Richter and Burrows (2002), Leue et al. (2001) and Hild et al. (2002), the albedo effect of underlying clouds can increase the NO_2 signal. Therefore, a reprocessing of the GOME NO_2 VTCs is carried out using an assumed NO_2 layer, the CTH, and the structure of the cloud cover. A closed cloud cover is assumed in the reprocessing version A. In version B, cloud mask information is used and the total tropospheric column (where cloud free) and above-cloud columns are combined. On the basis of preliminary trajectory calculations, the NO_2 is assumed to occur in a layer between 4000 and 6000 m a.s.l., whereas for standard pro-

cessing an a priori NO_2 profile with a constant mixing ratio in the lowermost 1.5 km of the troposphere is used (Richter and Burrows, 2002). For the underlying cloud cover, a height of 3000 m is assumed (which is accordance with live cams in the Alps). In fact, both the real vertical NO_2 distribution and the CTH are not exactly known, but an inaccurate estimation of this heights turned out to be not very critical. The two reprocessing scenarios A and B yielded quite similar column values as shown in Table 1. Furthermore, the reprocessing results in distinctly lower values than the standard processing, which is due to the above mentioned albedo effect of the clouds (Richter and Burrows, 2002; Leue et al., 2001; Hild et al., 2002). For the further analysis, the overall cloudy case is used.

4.2 Meteorological situation

After a frontal passage on 13 February, a high pressure system installed over southern England and moved slowly to the east, causing the inflow of dry continental polar air to Switzerland during 14–16 February (from Alpine Weather Statistics (MeteoSwiss, 1985)). The flat pressure distribution associated with the high pressure system led to stagnating air over middle Europe. On 16 February, a cold-front formed over north-eastern Europe (Figs. 3b and 4) and moved southward, developing to an occlusion during 17 February (Figs. 3d and 4).

Cold-fronts are often associated with lightning activity, the latter being known to be an in-situ source of NO_x in the free troposphere (e.g. Huntrieser et al., 2002). During the time of our case study, however, no lightning activity was recorded (www.wetterzentrale.de/topkarten/tkbeoblar.htm), and NO_2 production by lightning can, therefore, be excluded.

Table 1. GOME NO_2 vertical tropospheric column densities (VTCs) for the standard processing and the two reprocessing scenarios A and B. The NO_2 VTCs are the average values for the two pixel groups shown in Fig. 3c.

	standard processing	reprocessing A	reprocessing B
NO_2 profile	standard a priori profile, constant mixing ratio in the lowermost 1.5 km (Richter and Burrows, 2002)	NO_2 layer between 4000 and 6000 m a.s.l.	NO_2 layer between 4000 and 6000 m a.s.l.
cloud cover	–	closed cloud cover	partly cloudy
Cloud top height	–	3000 m a.s.l.	3000 m a.s.l.
NO_2 VTCs [$\times 10^{15}$ molec cm^{-2}]	38 (pixel group 1) 64 (pixel group 2)	13 (pixel group 1) 17.5 (pixel group 2)	12 (pixel group 1) 16.5 (pixel group 2)
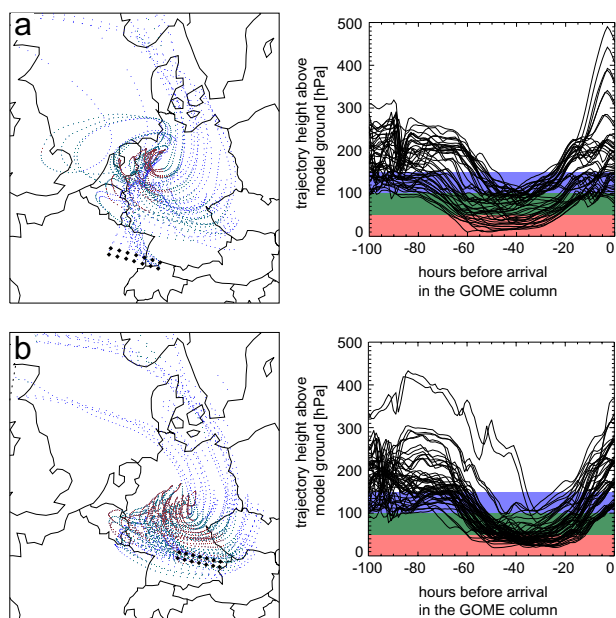
Fig. 5. Backward trajectories arriving on 17 February 2001, 9:00 UTC, in the two GOME pixel groups 1 **(a)** and 2 **(b)** defined in Fig. 3c. The coloured dots mark hourly trajectory time steps with a trajectory height above model ground of less than 150 hPa (blue), less than 100 hPa (green) and less than 50 hPa (red), respectively. For clarity, in the horizontal projections, only trajectories with a distance from ground of less than 100 hPa for at least one hourly time step are shown and trajectory points exceeding 150 hPa ground distances are omitted. The source regions of the detected NO_2 are likely to be located where the trajectories reside near the ground (red dots).

4.3 Backward trajectories – NO_2 source

The source region of the air pollution detected by the GOME instrument is analysed with backward trajectories (Fig. 5), focusing on the two NO_2 pixel groups (each composed of two GOME pixels as defined in Fig. 3c) over the border triangle of France, Germany and Switzerland (pixel group 1) and over south-eastern Germany (pixel group 2).

The trajectories indicate that the air masses arriving in the GOME columns are advected from western directions above the Northern Atlantic. They descend over Southern Scandinavia and the North Sea and subsequently turn clockwise over the region of the Netherlands, Belgium and Germany. This is a result of the presence of the high pressure system which installed over Europe before the frontal passage (Fig. 4). Near the ground, the vertical distribution of the trajectories is investigated in detail, because the residence time of an air parcel within the PBL allows the uptake of anthropogenic NO_2. For better identification of the potential source regions, only trajectories residing at a ground distance of less than 100 hPa for at least one (hourly) time step are considered in Fig. 5. Further, in the horizontal projections, time steps along these trajectories are omitted when their distance from ground exceeds 150 hPa. The potential source regions are most likely located where the trajectories travel near the ground, the latter indicated in Fig. 5 by trajectory time steps below 50 hPa ground distance. Comparing these regions with the GOME NO_2 VTCs on 16 February (Fig. 3a) shows a convincing coincidence between the regions with high NO_2 VTCs and the potential source regions. For 15 February, no GOME track covering the appropriate region is available. The narrow spatial distances of the hourly time steps (red dots in Fig. 5) show that the air was rather stagnant during 15 and 16 February. As a result, the air parcels were exposed to NO_x emissions for several hours in the highly populated region of the Netherlands, Belgium, Central Germany and the Ruhr area, the latter known to be one of the European hot spot regions concerning NO_2 pollution (Leue et al., 2001; Beirle et al., 2003; Konovalov, 2004). The air mass trajectories then exhibit a sudden movement to southern direction associated with frontal uplifting (Fig. 5). These air masses are highly likely to be responsible for the enhanced NO_2 in the pixel groups 1 and 2. The near-ground pollution reaches heights of up to 500 hPa above surface pressure (Fig. 5). This corresponds to lifting up to up to 5000 m above model ground. Even higher levels were reached by air formerly travelling at a ground distance of more than 100 hPa.

Comparing the backward calculations for GOME pixel groups 1 and 2 indicates that the air from pixel group 2 over south-eastern Germany is more affected by polluted PBL air,
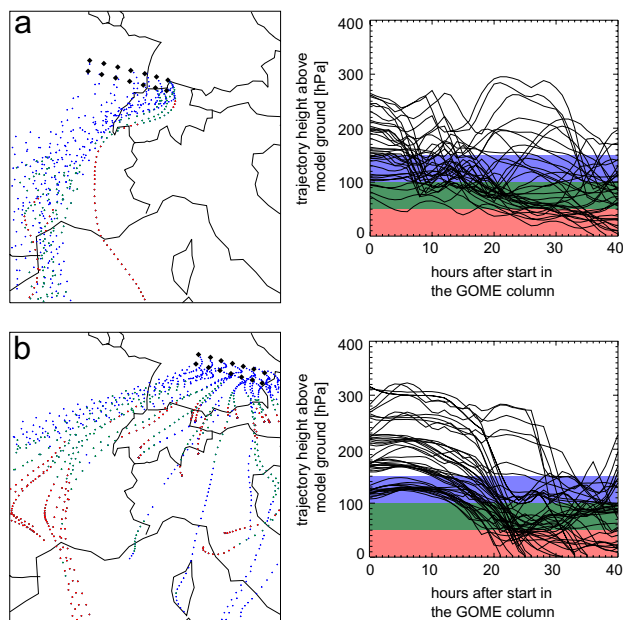
Fig. 6. The forward trajectories of the two GOME pixel groups 1 and 2 (defined in Fig. 3c) starting on 17 February 2001, 9:00 UTC, indicate the polluted air masses proceed to Switzerland and the Alpine region and further to south-west.

Fig. 7. NO$_2$ mixing ratios measured at the NABEL ground stations Chaumont, Rigi and Taenikon and at the high-alpine site at Zugspitze in February 2001.

because the density of the trajectories at less than 50 hPa is higher, and their uplifting takes place later. This explains the higher NO$_2$ VTCs in these GOME columns.

4.4   Forward trajectories – impact in the Alpine region

The forward trajectories show that the polluted air masses detected by GOME move to the Alpine region including Switzerland (Fig. 6). For both GOME pixel groups, the forward trajectories' distance to the ground decreases again. This is explained by both an effective subsidence and the increasing altitude of the ground in southern direction. The air masses reach heights below 50 hPa over the Alpine region (Fig. 6). The forward trajectories from GOME pixel group 1 stay relatively bundled and reach Switzerland in its north-western part. The trajectories from GOME pixel group 2, however, show a much larger spread and the polluted air reaching Switzerland can therefore be expected to be more diluted.

4.5   In-situ measurements in the Alpine region

The February 2001 time series of NO$_2$ measurements from the NABEL and Zugspitze stations indicate several events with high NO$_2$, the two most outstanding ones around 7–8 and 17–18 February (Fig. 7). The highest NO$_2$ mixing ratio of this month was measured in the evening on 17 February at the Rigi station with a value of 30 ppb. The NO$_2$ measurements at Chaumont and Zugspitze reached their maximum
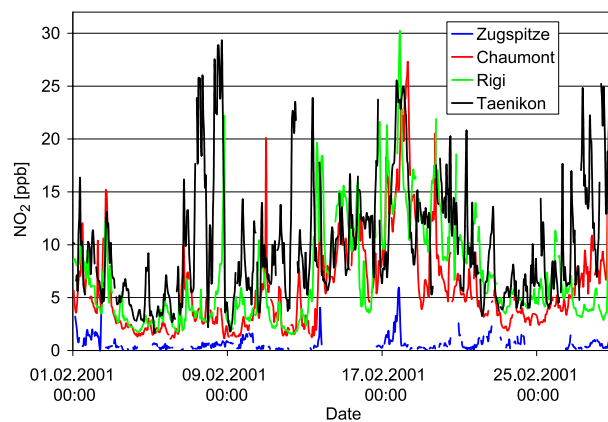
values at the same time with 27 ppb and 6 ppb, respectively. At the Taenikon station, the highest value was measured on 8 February (29 ppb), but the value on the evening of 17 February is, nevertheless, a distinct event with 26 ppb NO$_2$. What makes the event on 17–18 February special is the fact that all four stations show an almost simultaneous and significant increase in their nitrogen dioxide mixing ratios. This is in contrast to the event on 7–8 February, when very high NO$_2$ values are limited to Taenikon. There, local pollution events are frequent due to the relatively near highway and the inversion layer above the Swiss Plateau which increases pollution concentrations especially in winter.

The simultaneous pollution event on 17 and 18 February and the similar mixing ratios at the Swiss sites cannot be explained by local sources, because these are strongly different in the north of each of the considered measurement stations. Furthermore, thermal uplifting, which is typical for elevated sites, is not likely to occur during the night and early morning hours, when the maximum NO$_2$ mixing ratios were observed. Thus, the higher NO$_2$ amounts measured at the elevated stations must be caused by larger scale meteorological transport of pollution. It is noteworthy that the maximum NO$_2$ mixing ratios of 26 ppb measured in Taenikon, 27 ppb at Chaumont and 30 ppb at Rigi are quite similar, even though the annual mean NO$_2$ amounts show a pronounced decrease with increasing height (Taenikon: 7.0 ppb, Rigi: 4.8 ppb, Chaumont: 3.7 ppb (BUWAL, 2002)). These similar mixing ratios indicate a rather well mixed and extended air mass, the latter additionally confirmed by the simultaneous increasing mixing ratio at Zugspitze which is located about 290 km away from Rigi. These findings agree well with the above described air masses that have taken up pollution over an extended region and having been transported over mesoscale distances of several hundred kilometres.
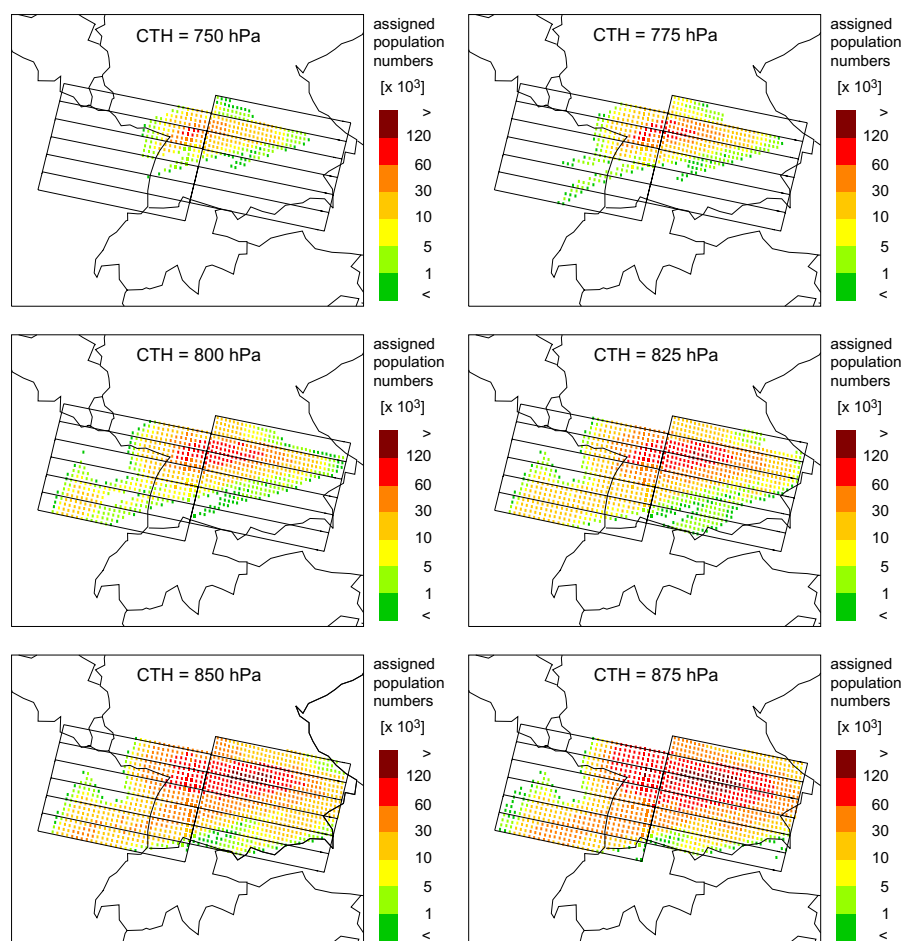
Fig. 8. Population numbers (assigned to the backward trajectories as a proxy for NO_x emissions) added up above different cloud top heights (CTH) between 750 hPa and 875 hPa to a 2-dimensional proxy for the NO_2 distribution above the clouds.

4.6 Transport model

4.6.1 Effective cloud top height and conversion with GOME observations

Our method proposed in Sect. 3.2 and illustrated in the flow chart of Fig. 2 is used to model the transport of NO_2 for this case study. The core element of it is the conversion of population numbers assigned to the trajectories as a proxy for NO_2 to number of NO_2 molecules considering the GOME NO_2 VTCs and the CTH_{eff}. As pointed out in Sect. 3.2.2, the latter is defined to be the CTH for which the modelled above-cloud pollution (proxy VTCs) best reproduces the detected pollution from GOME (NO_2 VTCs). Figure 8 illustrates an intermediate step where the population numbers assigned to the trajectories are added up above different CTH ranging between 750 and 875 hPa. This results in a 2-dimensional proxy for the NO_2 distribution above the clouds. Especially when the CTH is in the range of 800 to 875 hPa (which is lower than the real CTH), the modelled NO_2 distribution re-

sembles the GOME observation (Fig. 3c). The band structure of high NO_2 present in Fig. 8 agrees with the shape of the occlusion in Fig. 4 and indicates the uplift of previously ground-near pollution.

Summing the population numbers from Fig. 8 for each of the 12 considered GOME pixel locations (Fig. 3c) yields the NO_2 proxy VTCs. They are related to the appropriate NO_2 VTCs from GOME in order to determine the adequate CTH_{eff} for the further calculation. Figure 8 already indicates that the CTH_{eff} must be located at a lower altitude because the pollution distribution detected from GOME (Fig. 3c) seems to be better reproduced at these CTHs. For a CTH of, e.g. 750 hPa, a poor linear fit between the two quantities can be expected: for some GOME pixel locations, no NO_2 proxy is found above the clouds although the appropriate GOME columns show an enhanced NO_2 amount (Figs. 8 and 3c). Figure 9 shows the scatter plot between the two quantities for the CTH located at 850 hPa. For this CTH, a relatively good correlation and no offset is found between the proxy VTCs and the GOME NO_2 VTCs although a constant
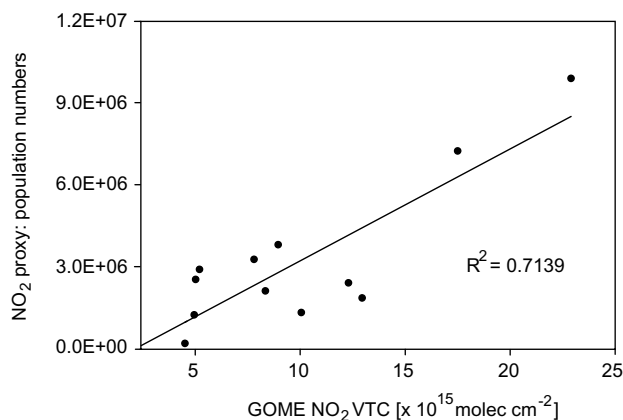
Fig. 9. Scatter plot and linear fit between vertical column proxy (population numbers) and appropriate GOME NO_2 VTCs for a CTH of 850 hPa.
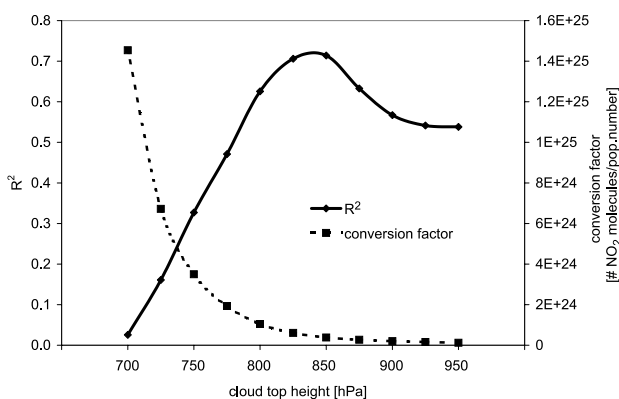

Fig. 10. Explained variance R^2 of the linear fit between the proxy vertical column densities and the GOME NO_2 VTCs (solid line) and the respective conversion factors (dashed line) for different CTHs.

Fig. 11. **(a)** NO_2 mixing ratios measured at the Zugspitze station during the investigated episode (black) and model results for the advected additional NO_2 for an NO_2 lifetime of 24 h (red) and of 12 h (green). **(b)** Measured NO_2 mixing ratios (black) and model results for different assumptions on the planetary boundary layer (PBL) height. In order to simplify the visual assessment of the figure, the time shift of the modelled curves is neglected.

CTH has been assumed. This indicates the latter assumption to be not too far away from reality. This is also confirmed by an inspection of more recent satellite data (KNMI, personal communication) indicating that all the CTHs of the individual pixels lie in a range of within 8% around the mean CTH over the 12 considered GOME column locations of 693.5 hPa, the latter being very close to the assumption made in Sect. 4.1. Figure 10 summarises the explained variances R^2 of the linear fits for different CTHs. As the R^2-curve culminates at about 840 hPa, we use this CTH_{eff} as the relevant level for our further calculation and use the 825 and 850 hPa levels as the confidence interval.

The conversion factor is the ratio between the sum of the 12 GOME NO_2 VTCs (Fig. 3c) and the sum of the respective 12 proxy VTCs (calculated above CTH_{eff}). The conversion function showing the conversion factor for different CTHs (Fig. 10) indicates that small changes around 840 hPa do not have a large impact on the results. With the conversion
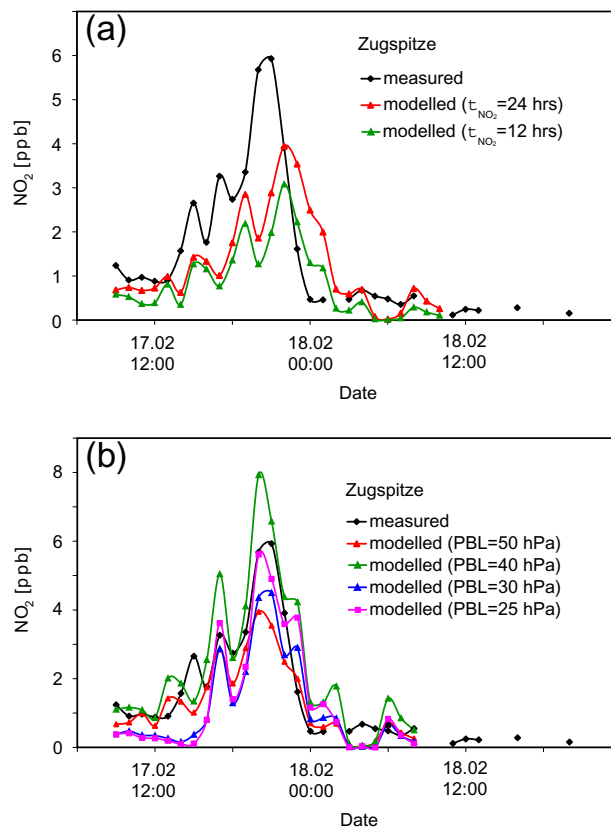
factor associated with 840 hPa, the population number of every trajectory is converted to an NO_2 amount, which further propagates along the forward trajectory.

4.6.2 Comparing in-situ measurements and modelled impact

Below, the modelled NO_2 concentrations are compared with the actual measurements at the ground stations. As pointed out in Sect. 3.2.3 the trajectories are defined to reach a ground measurement site as soon as they travel near the ground. The definition of the near-ground level, however, is not straightforward. The representation of the complex topography in the Alpine region can be thought to be relatively poor in the coarse resolved ECMWF model. Generally, trajectory modelling requires a height of a station to be not too far from the model topography for realistic results. For the present episode, the ECMWF model ground has been 960, 947, 906 and 875 hPa for Taenikon (real surface pressure in winter
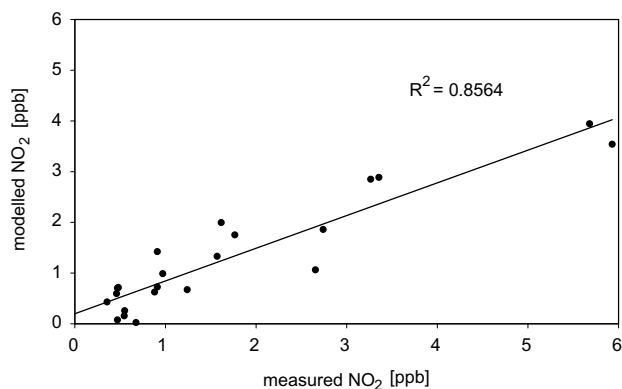
Fig. 12. Scatter plot and linear fit between the NO_2 concentration measured at the ground station Zugspitze and the respective modelled NO_2 mixing ratios for an assumed PBL height of 50 hPa (and an NO_2 lifetime of 24 h).

around 950 hPa), Chaumont (890 hPa), Rigi (900 hPa) and Zugspitze (700 hPa), respectively. For the first three stations, the box extension in which the trajectories are taken into account is defined to be up to 50 hPa distance from model ground. For the Zugspitze, however, the model ground differs much more from the real height. Taking the real height of the site could thus lead to errors, because trajectories representing the free troposphere would be regarded as being representative for the Zugspitze. Therefore, the box representing the Zugspitze station is chosen to be located in distance of between 50 hPa and 100 hPa from model ground.

The model results for Zugspitze are shown, together with the measured time series of NO_2, in Fig. 11. The modelled NO_2 mixing ratios match the measured series surprisingly well (Fig. 11a). The measured variations in the NO_2 mixing ratio are reproduced and the modelled maximum value of about 4 ppb is in the order of the measured value of 6 ppb. Assuming that no local pollution occurred at this high-alpine site, the bulk of the 6 ppb NO_2 can be considered as being due to frontal transport. This implies, that the model approach somewhat underestimates the transported NO_2. The time shift of the modelled relative to the measured time series of about 1 to 2 h is most likely explained by inaccuracies in the near-ground trajectories.

Sensitivity studies concerning the average NO_2 lifetime and the PBL height have been performed. Figure 11a includes the time series modelled for an average NO_2 lifetime of 12 and of 24 h for Zugspitze. The comparison shows that this quantity has not a major impact on the results. Further calculations (not shown) indicated that for the other investigated sites, the differences due to different lifetimes are even smaller. Following the arguments pointed out in Sect. 3.2.4, an average lifetime of 24 h is chosen for the further calculation.

The assumed PBL height in the NO_2 source region has been varied between 25 and 50 hPa. In Fig. 11b, the time shift is adjusted for better visualisation. The absolute values depend somewhat on the assumed height of the PBL and also on the vertical resolution of the trajectory model (in our case 25 hPa). The time series calculated for a 40 hPa PBL indicate higher concentrations at the Zugspitze compared to the 50 hPa PBL run. This is expected because a lower number of polluted trajectories arrive in the GOME columns at an altitude above the CTH_{eff}. Thus, the conversion factor increases. Further decreasing the PBL height leads to lower pollution also below the clouds which explains the decrease in the modelled concentrations for an assumed PBL of 30 hPa compared to the 40 hPa run. The best estimate for the PBL height is chosen via correlating the different resulting time series with the measured concentrations with the time shift adjusted. The best correlation is found for a PBL height of 50 hPa (Fig. 12). Defining a near-ground layer of 50 hPa corresponds to a PBL height of about 500 m. This is rather high for winter conditions investigated in this episode. However, near the ground, trajectories are less accurate than at higher levels. This might be a reason for the best result emanating from modelling with a rather high PBL. Furthermore, mixing processes during the frontal movement associated with the southward transport described here complicates the proper definition of a PBL height.

Altogether, changing parameters such as the average NO_2 lifetime and the PBL height does not change the results strongly (also valid for the other stations, not shown) because the conversion in the GOME columns compensates to some extent for different starting conditions. Thus, the results are relatively stable and indicate a successful use of the suggested method for this transport episode.

Figure 13 illustrates the measured (black) and modelled (red) NO_2 time series for all the stations investigated in this study. Besides the result for the CTH_{eff} located at 840 hPa, the modelled concentrations for the two neighbouring levels with trajectory calculations in 850 and 825 hPa are additionally shown as a confidence interval. The model output for Taenikon is less correlated with the measurement than seen for the Zugspitze station. At the beginning of the episode, the increasing mixing ratios are well shown by the model results, but the nearly constant values during the night are somewhat overestimated. However, the time range of the overall event is reproduced well and the order of magnitude of the NO_2 mixing ratio is matched. For the two elevated sites at Rigi and Chaumont, the time series modelled for the grid cells corresponding to the sites did not explain the measured NO_2 time series adequately. Taking into account adjacent grid cells, the time series found there match the measured mixing ratios much better, which might be due to uncertainties in the near-ground trajectories. The latter explanation is additionally supported by the fact that for both stations, the corresponding adjacent grid cells are found to be shifted towards the Swiss Plateau. This favours the following explanation:
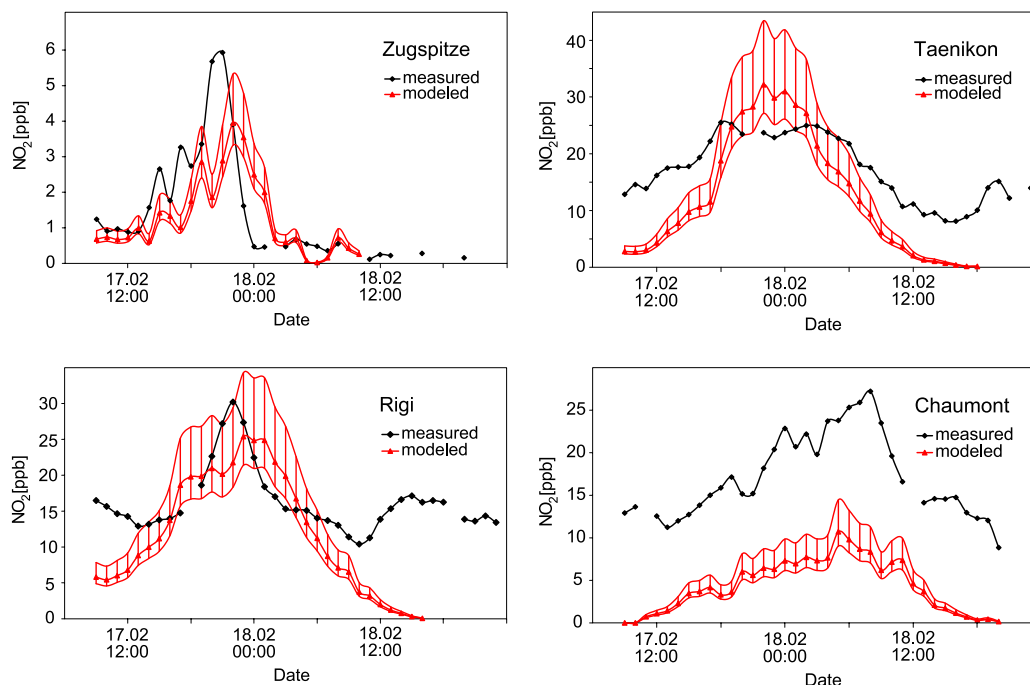
Fig. 13. NO_2 mixing ratios measured during the investigated episode (black) and results of the model assessment of the advected additional NO_2 (red). The thick red curve corresponds to the optimal CTH_{eff} at 840 hPa, the thin curves from the adjacent (trajectory) levels in 825 (upper curve) and 850 hPa (lower curve) are shown as a confidence interval. For the Zugspitze and Taenikon stations, the time series from the grid cells containing the measurement sites are used, whereas for Rigi and Chaumont, adjacent grid cells show more reliable results (see text).

the air mass flow is approximately parallel to the mountain ridges on which the two stations are located (the Jura Mountains for Chaumont and the foothills of the Alps for Rigi, Figs. 1 and 6). However, the complex Swiss topography strongly affecting the flow is not properly resolved in the ECMWF model with a resolution of $1° \times 1°$, displacing the near-ground trajectories somewhat. The modelled NO_2 in the appropriate adjacent grid cells explain the shapes of the measured NO_2 time series at Rigi and Chaumont quite reasonable although for the Chaumont station, the modelled mixing ratios are distinctly lower than the measured values. A reason for that could be that the Chaumont station is most affected by air masses from pixel group 1 (Figs. 1, 3c, and 6). Figure 6 indicates that the air from pixel group 2 has to cover a larger distance to reach this most western station and can, therefore, be expected to have a minor influence. The colours of pixel group 1 in Fig. 8 further show that the NO_2 proxy for these two pixels might be somewhat underestimated by our method, because for this pixel group with the second highest column values (Fig. 3c), we would expect higher population numbers. This underestimation is probably due to the assumption of a cloud cover with a uniform height.

During the investigated episode, roughly 50 to 90% of the measured NO_2 are found to be caused by transboundary transport. This seems plausible taking into account that the

mean NO_2 mixing ratios are much lower. The latter are determined by averaging the NO_2 mixing ratios over the February months of the years 1999 to 2001 for the four stations (with the investigated period from 17 February, 0:00 MET, to 18 February, 12:00 MET, excluded). Typical night time NO_2 mixing ratios from 0.5 ppb at Zugspitze to about 5 ppb for the elevated sites at Rigi and Chaumont are found. Only the Swiss Plateau station Taenikon shows evening mixing ratios exceeding 10 ppb.

Altogether we conclude from the comparison of the measured with the modelled NO_2 mixing ratios that the GOME NO_2 VTCs combined with our model can explain the exceptional events with high mixing ratios measured at the four sites and that the proposed method using above-cloud NO_2 detected from space can successfully be applied.

5 Summary and conclusions

A method is presented to exploit enhanced tropospheric GOME NO_2 measurements above extended cloud covers together with a trajectory based analysis to quantitatively assess air pollution transport. A NO_2 proxy is assumed to be proportional to the population distribution in the source region and is accumulated along ground-near trajectories considering an assumed average NO_2 lifetime. After arriving

at the locations of the GOME columns, the proxy vertical tropospheric column densities (VTCs) are calculated above different cloud top heights (CTHs). Comparing the latter with the GOME NO$_2$ VTCs allows choosing the most appropriate effective cloud top height (CTH$_{eff}$) where the pollution distribution from GOME is best reproduced by the model. Relating the proxy VTCs with the GOME NO$_2$ VTCs yields a factor for converting the proxy to number of NO$_2$ molecules. Because the transport model covers the whole tropospheric columns, this results in an implicit estimate of the NO$_2$ distribution including its sub-cloud part. Further tracing the air masses with forward trajectories allows the estimation of pollution transport to other areas.

In a case study, the origin and impact of air pollution observed from the GOME instrument on 17 February 2001 above a cloud cover is investigated. Trajectory studies reveal that polluted boundary layer air was lifted up by a frontal system. This led to nitrogen dioxide being located within and/or above an extended cloud cover and therefore being detectable by the GOME instrument. The source region of the NO$_2$ pollution is identified as the central part of Germany, the Ruhr area, and adjacent regions in the Netherlands and Belgium. Forward trajectory calculations indicate the subsequent movement of the polluted air masses to the Alpine region and predict that measurement stations in Switzerland and southern Germany are affected by the frontal transported NO$_2$. Rural in-situ measurements of enhanced NO$_2$ mixing ratios during the night confirm the prediction.

The NO$_2$ transport to the Alpine area is modelled using the proposed method and compared with the ground-based measurements. The model successfully reproduced the measured time series and shows that at least 50% of the NO$_2$ peak mixing ratios measured at the stations during the frontal passage can be attributed to transboundary transport. It is further demonstrated that the suggested method to convert the NO$_2$ proxy into NO$_2$ concentrations using CTH$_{eff}$ and the appropriate above-cloud NO$_2$ VTCs from GOME is stable in terms of changing parameters such as the average NO$_2$ lifetime and the assumed boundary layer height.

The study shows the potential of pollution detected from space-borne spectrometers above cloudy scenes. For compounds measured in the visible spectral range (as, e.g. NO$_2$ from GOME) this means that the lowest and often most polluted part of the troposphere is shielded from view. However, retrievals above clouds might be of better quality because of the enhanced sensitivity of satellite measurements above a strong reflector. The synergistic use of pollution detected above clouds and transport models in order to model pollution transport to ground stations is demonstrated in this study. It is planned to further improve the method by applying individual CTHs for every pixel (recently provided with satellite data). The enhanced spatial resolution of instruments such as SCIAMACHY further allows accounting for inhomogeneities in the CTH. It is intended to apply the described method on an extended data set of cloudy scenes observed from GOME and SCIAMACHY. This could further contribute to the issue of transboundary pollution transport and its impact at remote measurement sites.

References

Beirle, S., Platt, U., Wenig, M., and Wagner, T.: Weekly cycle of NO$_2$ by GOME measurements: a signature of anthropogenic sources, Atmos. Chem. Phys., 3, 2225–2232, 2003, **SRef-ID: 1680-7324/acp/2003-3-2225**.

Bethan, S., Vaughan, G., Gerbig, C., Volz-Thomas, A., Richer, H., and Tiddeman, D. A.: Chemical air mass differences near fronts, J. Geophys. Res., 103, 13 413–13 434, 1998.

Boersma, K. F., Eskes, H. J., and Brinksma, E. J.: Error analysis for tropospheric NO$_2$ retrieval from space, J. Geophys. Res., 109, art. no. D04311, doi:10.1029/2003JD003962, 2004.

Brasseur, G. P.: Atmospheric chemistry in a changing world, Springer Verlag, Berlin, 2003.

Burrows, J. P., Weber, M., Buchwitz, M., Rozanov, V., Ladstätter-Weissenmayer, A., Richter, A., DeBeek, R., Hoogen, R., Bramstedt, K., Eichmann, K. U., Eisinger, M., and Perner, D.: The global ozone monitoring experiment (GOME): Mission concept and first scientific results, J. Atmos. Sci., 56, 151–175, 1999.

BUWAL: NABEL – Luftbelastung 2001, Schriftenreihe Umwelt Nr. 343, 2002.

Dentener, F. J. and Crutzen, P. J.: Reaction of N$_2$O$_5$ on tropospheric aerosols: impact on the global distributions of NO$_x$, O$_3$ and OH, J. Geophys. Res., 98, 7149–7163, 1993.

Dickerson, R. R., Stedman, D. H., and Delany, A. C.: Direct measurements of ozone and nitrogen-dioxide photolysis rates in the troposphere, J. Geophys. Res., 87, 4933–4946, 1982.

Donnell, E. A., Fish, D. J., Dicks, E. M., and Thorpe, A. J.: Mechanisms for pollutant transport between the boundary layer and the free troposphere, J. Geophys. Res., 106, 7847–7856, 2001.

EMPA: Technischer Bericht zum Nationalen Beobachtungsnetz für Luftfremdstoffe (NABEL), Duebendorf, 2002.

Forrer, J., Rüttimann, R., Schneiter, D., Fischer, A., Buchmann, B., and Hofer, P.: Variability of trace gases at the high-Alpine site Jungfraujoch caused by meteorological transport processes, J. Geophys. Res., 105, 12 241–12 251, 2000.

Hild, L., Richter, A., Rozanov, V., and Burrows, J. P.: Air mass factor calculations for GOME measurements of lightning-produced NO$_2$, Adv. Space Res., 29, 1685–1690, 2002.

Hov, O. and Flatoy, F.: Convective redistribution of ozone and oxides of nitrogen in the troposphere over Europe in summer and fall, J. Atmos. Chem., 28, 319–337, 1997.

Huntrieser, H., Feigl, C., Schlager, H., Schroder, F., Gerbig, C., van Velthoven, P., Flatoy, F., Thery, C., Petzold, A., Holler, H., and Schumann, U.: Airborne measurements of NO_x, tracer species, and small particles during the European lightning nitrogen oxides experiment, J. Geophys. Res., 107, art. no. 4113, doi:10.1029/2000JD000209, 2002.

Jacob, D. J., Crawford, J., Kleb, M. M., Connors, V. S., Bendura, R. J., Raper, J. L., Sachse, G. W., Gille, J., Emmons, L., and Heald, J. C.: Transport and Chemical Evolution Over the Pacific (TRACE-P) mission: Design, execution, and first results, J. Geophys. Res., 108, art. no. 9000, doi:10.1029/2002JD003276, 2003.

Jaeglé, L., Jacob, D. J., Wang, Y., Weinheimer, A. J., Ridley, B. A., Campos, T. L., Sachse, G. W., and Hagen, D. E.: Sources and chemistry of NO_x in the upper troposphere over the United States, Geophys. Res. Lett., 25, 1705–1708, 1998.

Konovalov, I. B., Beekmann, M., Vautard, R., Burrows, J. P., Richter, A., Nüss, H., and Elansky, N.: Comparison and evaluation of modelled and GOME measurement derived tropospheric NO_2 columns over Western and Eastern Europe, Atmos. Chem. Phys. Discuss., 4, 6503–6558, 2004,
SRef-ID: 1680-7375/acpd/2004-4-6503

Kramm, G., Dlugi, R., Dollard, G. J., Foken, T., Mölders, N., Müller, H., Seiler, W., and Sievering, H.: On the dry deposition of ozone and reactive nitrogen species, Atmos. Environ., 29, 3209–3231, 1995.

Kunhikrishnan, T., Lawrence, M. G., von Kuhlmann, R., Richter, A., Ladstätter-Weissenmayer, A., and Burrows, J. P.: Analysis of tropospheric NO_x over Asia using the model of atmospheric transport and chemistry (MATCH-MPIC) and GOME-satellite observations, Atmos. Environ., 38, 581–596, 2004.

Leue, C., Wenig, M., Wagner, T., Klimm, O., Platt, U., and Jahne, B.: Quantitative analysis of NO_x emissions from Global Ozone Monitoring Experiment satellite image sequences, J. Geophys. Res., 106, 5493–5505, 2001.

MeteoSwiss: Alpine Weather Statistics (Alpenwetterstatistik - Witterungskalender: Beschreibung der einzelnen Parameter), MeteoSwiss, Switzerland, 1985.

Nakamura, K., Kondo, Y., Chen, G., Crawford, J. H., Takegawa, N., Koike, M., Kita, K., Miyazaki, Y., Shetter, R. E., Lefer, B. L., Avery, M., and Matsumoto, J.: Measurement of NO_2 by the photolysis conversion technique during the Transport and Chemical Evolution Over the Pacific (TRACE-P) campaign, J. Geophys. Res., 108, art. no. 4752, doi:10.1029/2003JD003712, 2003.

Parrish, D. D., Murphy, P. C., Albritton, D. L., and Fehsenfeld, F. C.: The measurement of the photo-dissociation rate of NO_2 in the atmosphere, Atmos. Environ., 17, 1365–1379, 1983.

Richter, A. and Burrows, J. P.: Tropospheric NO_2 from GOME measurements, Adv. Space Res., 29, 1673–1683, 2002.

Seinfeld, J. H. and Pandis, S. N.: Atmospheric chemistry and physics – from air pollution to climate change, John Wiley & Sons, New York, 1998.

Spichtinger, N., Wenig, M., James, P., Wagner, T., Platt, U., and Stohl, A.: Satellite detection of a continental-scale plume of nitrogen oxides from boreal forest fires, Geophys. Res. Lett., 28, 4579–4582, 2001.

Stohl, A., Eckhardt, S., Forster, C., James, P., and Spichtinger, N.: On the pathways and timescales of intercontinental air pollution transport, J. Geophys. Res., 107, art. no. 4684, doi:10.1029/2001JD001396, 2002.

Stohl, A., Huntrieser, H., Richter, A., Beirle, S., Cooper, O. R., Eckhardt, S., Forster, C., James, P., Spichtinger, N., Wenig, T., Wagner, T., Burrows, J. P., and Platt, U.: Rapid intercontinental air pollution transport associated with a meteorological bomb, Atmos. Chem. Phys., 3, 969–985, 2003,
SRef-ID: 1680-7324/acp/2003-3-969.

Umweltbundesamt: Jahresbericht 2001 aus dem Messnetz des Umweltbundesamtes, 69, Berlin, 2002.

Warneck, P.: Chemistry of the natural atmosphere, second edition, Academic Press, London, 2000.

Wenig, M., Spichtinger, N., Stohl, A., Held, G., Beirle, S., Wagner, T., Jahne, B., and Platt, U.: Intercontinental transport of nitrogen oxide pollution plumes, Atmos. Chem. Phys., 3, 387–393, 2003,
SRef-ID: 1680-7324/acp/2003-3-387.

Wernli, H. and Davies, H. C.: A Lagrangian-based analysis of extratropical cyclones. 1. The method and some applications, Q. J. R. Meteo., 123, 467–489, 1997.

Wiegand, A. N. and Bofinger, N. D.: Review of empirical methods for the calculation of the diurnal NO_2 photolysis rate coefficient, Atmos. Environ., 34, 99–108, 2000.

Winer, A. M. and Biermann, H. W.: Long path length differential optical-absorption spectroscopy (DOAS) measurements of gaseous HONO, NO_2 and HCHO in the California south coast air basin, Res. Chem. In., 20, 423–445, 1994.

Wunderli, S. and Gehrig, R.: Influence of temperature on formation and stability of surface PAN and ozone – a 2-year field-study in Switzerland, Atmos. Environ., 25, 1599–1608, 1991.

Zellweger, C., Ammann, M., Hofer, P., and Baltensperger, U.: NO_y speciation with a combined wet effluent diffusion denuder - aerosol collector coupled to Ion chromatography, Atmos. Environ., 33, 1131–1140, 1999.

Zellweger, C., Forrer, J., Hofer, P., Nyeki, S., Schwarzenbach, B., Weingartner, E., Ammann, M., and Baltensperger U.: Partitioning of reactive nitrogen (NO_y) and dependence on meteorological conditions in the lower free troposphere, Atmos. Chem. Phys., 3, 779–796, 2003,
SRef-ID: 1680-7324/acp/2003-3-779.